uplift at 48 to 46.4 Ma [M. A. House and K. V. Hodges, *Geology* **22**, 1007 (1994)].
10. A. Hietanen, *U.S. Geol. Surv. Prof. Pap.* **344-B** (1963).
11. Anorthite (±kyanite) + H_2O is stable relative to margarite (±clinozoisite) + quartz only at temperatures of at least 515° ± 25°C (4 kbar) [B. Storre and K. H. Nitsch, *Contrib. Mineral. Petrol.* **43**, 1 (1974); T. H. Brown, R. G. Berman, E. H. Perkins, *Comput. Geosci.* **14**, 279 (1988)]. Only high-temperature (≥500°C) water-rock interaction will lead to isotopic exchange of feldspar without also forming hydrous phases (*1*).
12. H. P. Taylor Jr., *N.Y. State Mus. Sci. Serv. Mem.* **18**, 111 (1969).
13. Andesine and anorthite were separated using dense liquids. Mineral and whole-rock samples were analyzed using conventional methods of BrF_5 reaction and isotope ratio mass spectrometry [R. N. Clayton and T. K. Mayeda, *Geochim. Cosmochim. Acta* **27**, 43 (1963)]. Isotope ratios are reported in delta notation where $\delta^{18}O = [(^{18}O/^{16}O \text{ sample})/(^{18}O/^{16}O \text{ standard}) - 1]1000$ per mil relative to the V-SMOW standard. In situ oxygen isotope analyses were obtained on a Cameca ims 4f SIMS using a low-energy electron gun for sample charge compensation, extreme energy filtering, and instrument conditions [L. R. Riciputi, B. A. Patterson, R. L. Ripperdan, *Int. J. Mass Spectrom. Ion Processes* **178**, 81(1998)]. SIMS results have external reproducibility of 0.6 to 1 per mil (1σ) for a spot diameter of ~30 μm.
14. Above 500°C, the oxygen isotope fractionation between water and plagioclase is <1 per mil [Y. Matsuhisa, J. R. Goldsmith, R. N. Clayton, *Geochim. Cosmochim. Acta* **43**, 1131 (1979)]. Isotopic compositions of bulk plagioclase samples in the Boehls Butte anorthosite indicate exchange with evolved meteoric-hydrothermal fluids having $\delta^{18}O$ in the range +5 to −8 per mil.
15. Y. F. Zheng, B. Fu, B. Gong, S. G. Li, *Eur. J. Mineral.* **8**, 317 (1996).
16. R. E. Criss and H. P. Taylor Jr., *Geol. Soc. Am. Bull.* **94**, 640 (1983).
17. The models considered diffusion from a stirred solution of limited volume into a sphere [A. C. Lasaga, *Kinetic Theory in the Earth Sciences* (Princeton Univ. Press, Princeton, NJ, 1998)] at 550°C. We used diffusion constants for wet andesine and wet anorthite [B. J. Giletti, M. P. Semet, R. A. Yund, *Geochim. Cosmochim. Acta* **42**, 45 (1978)] and for dry anorthite [S. C. Elphick, C. M. Graham, D. F. Dennis, *Contrib. Mineral. Petrol.* **100**, 690 (1988)]; the difference between dry and wet anorthite was used to scale and estimate dry andesine coefficients from wet andesine data. Diffusion coefficients were then rescaled for changes in confining pressure and f_{H_2O} [J. R. Farver and R. A. Yund, *Geochim. Cosmochim. Acta* **54**, 2953 (1990)]. For P_{H_2O} = 1 kbar, we used $D = 3.35 \times 10^{-15}$ cm^2 s^{-1}; for P_{H_2O} = 1 bar, we used $D = 3.2 \times 10^{-17}$ cm^2 s^{-1}; and for $P_{H_2O} = 0$, we used $D = 3.2 \times 10^{-22}$ cm^2 s^{-1}. The initial plagioclase composition was taken to be +5 per mil, with fluid compositions of −11 per mil (Fig. 2, top) or −16 per mil (Fig. 2, bottom), and a water:rock ratio = 10 (by weight).
18. K. J. Edwards and J. W. Valley, *Geochim. Cosmochim. Acta* **62**, 2265 (1998).
19. M. J. Kohn, *Am. Mineral.* **84**, 570 (1999).
20. C. I. Mora and K. Ramseyer, *Am. Mineral.* **77**, 1258 (1992).
21. P. M. Orville, *Am. J. Sci.* **272**, 234 (1972). The volume change of this reaction is especially large (~50%) if quartz is removed from the immediate site of reaction; only minor amounts of quartz are observed in the anorthosite, often within andesine megacrysts.
22. The rapid loss of grain boundary fluid followed by dry cooling has also been inferred in metacarbonate rocks [C. M. Graham, J. W. Valley, J. M. Eiler, H. Wada, *Contrib. Mineral. Petrol.* **132**, 371 (1998)].
23. M. A. House, K. V. Hodges, S. A. Bowring, *J. Metamorph. Geol.* **15**, 753 (1997).
24. Supported by NSF grant EAR-8922638 and an Oak Ridge Associated Universities Faculty Participation Program Fellowship to C.I.M., NSF grant EAR-9706077 to L.R.R., and the Office of Science, Basic Energy Sciences, U.S. Department of Energy under contract DE-ACO5-96OR22464 with Oak Ridge National Laboratory, which is managed by Lockheed Martin Energy Research Corporation.

16 July 1999; accepted 21 October 1999

Surfactant-Mediated Two-Dimensional Crystallization of Colloidal Crystals

Laurence Ramos,[1]* T. C. Lubensky,[1] Nily Dan,[2] Philip Nelson,[1] D. A. Weitz[1]†‡

Colloidal particles can form unexpected two-dimensional ordered colloidal crystals when they interact with surfactants of the opposite charge. Coulomb interactions lead to self-limited adsorption of the particles on the surface of vesicles formed by the surfactants. The adsorbed particles form ordered but fluid rafts on the vesicle surfaces, and these ultimately form robust two-dimensional crystals. This use of attractive Coulomb interaction between colloidal particles and surfactant structures offers a potential new route to self-assembly of ordered colloidal structures.

The self-assembly of colloidal particles is a promising route to materials synthesis that combines considerable flexibility in the choice of materials with the opportunity to create highly ordered structures on length scales from nanometers to micrometers. Self-assembled structures can form resilient coatings, templates for growth of ordered micro- and nanoporous materials (*1*), and even photonic devices (*2*–*4*). Self-assembly depends critically on thermal energy; the resultant motion allows particles to attain the optimum positions to create desired highly ordered structures.

To exploit thermal motion, great care must be taken in controlling the interaction energies between the particles themselves and between the particles and their surroundings. Thermally induced self-assembly typically requires repulsive or only very weakly attractive interactions. Strong attraction usually leads to the formation of highly disordered aggregates, rather than ordered colloidal crystal structures. Because of this, attractive Coulomb interactions, which are strong on thermal scales, are usually not effective in producing self-assembled, ordered structures. Thus, for example, when charge-stabilized colloidal particles are mixed with surfactants of the opposite charge, they typically destabilize and form disordered fractal aggregates (*5*) because the surfactant binds Coulombically to the particles. This process makes their surfaces hydrophobic and leads to strongly attractive interparticle interactions.

Because of this expectation of destabilization, few studies of mixtures of particles and oppositely charged surfactants have been reported. However, surfactants can self-assemble into a rich array of structures, and the possibility of the interaction of these structures with the oppositely charged colloidal particles is ignored in the disordered-aggregate scenario. Indeed, recent studies of mixtures of positively charged lipids with negatively charged DNA have shown that highly ordered structures can ensue (*6, 7*).

We report the unexpected formation of large colloidal crystals when aqueous charge-stabilized polystyrene latex particles are combined with a mixture of an oppositely charged and a neutral surfactant, which self-assemble into vesicles. Surprisingly, exclusively two-dimensional (2D) colloidal crystals are formed. Coulomb attractions cause the adsorption of particles onto the vesicle surfaces, which mediate the formation of 2D crystals. We propose a model that accounts for the observations made during several steps in the sequence resulting in the 2D crystals. This new route to self assembly may serve as a template for the synthesis of novel ordered structures.

We used a mixture of two surfactants: didodecyldimethylammonium bromide (DDAB), a cationic, double-chained amphiphile, and polyoxyethylene (9-10) *p-tert*-octyl phenol (Triton X-100, or TX), a nonionic, single-chained amphiphile. These surfactants have similar areas per polar head group (0.6 nm^2) and similar critical micelle concentrations (cmc) (*8*). Above the cmc, DDAB alone self-

[1]Department of Physics and Astronomy, University of Pennsylvania, 209 South 33rd Street, Philadelphia, PA 19104, USA. [2]Department of Chemical Engineering, Drexel University, Philadelphia, PA 19104, USA.

*Present address: Groupe de Dynamique des Phases Condensées, (CNRS-UMII) cc26, Université Montpellier II, place E. Bataillon, 34095 Montpellier Cedex 5, France.

†Present address: Department of Physics and Division of Engineering and Applied Sciences, Harvard University, Cambridge, MA 02138, USA.

‡To whom correspondence should be addressed. E-mail: weitz@deas.harvard.edu

assembles into bilayer vesicles (*9*), whereas TX alone forms micelles (*10*). We varied the molar fraction, x, of TX in the mixture; at small x, we expected TX to be incorporated into DDAB vesicles; at high x, we expected DDAB to be incorporated into TX micelles, and at intermediate x, we expected vesicles of DDAB mixed with TX, with the excess TX in micelles. To enhance vesicle formation, we often added a cosurfactant, octanol, in a fixed ratio of 0.35 by weight to the TX; this increased the range of x for vesicle formation (*11*). Sonicating for 30 min led to the formation of vesicles that ranged from one-tenth to several micrometers in diameter. To such a mixture, we added negatively charged polystyrene latex spheres (*12*) at volume fractions of about 0.5%. We observed the resultant structures with optical microscopy, using both phase and differential interference contrast.

When the total surfactant concentration was less than the cmc, the particles remain totally dispersed for all values of x. When the surfactant concentration was increased above the cmc, the particles still remained completely dispersed for $x = 1$, when only the nonionic TX was present. In contrast, at $x = 0$ (cationic DDAB the only species present above its cmc), large, disordered aggregates were observed. Completely unexpected behavior was observed for surfactant concentrations above the cmc and at intermediate values of x (*13*); large, ordered colloidal crystals formed (Fig. 1) that were always 2D and consisted of a single layer. Three-dimensional crystals were never observed. The crystals typically contained several hundred particles and possessed a few defects, such as vacancies, disclinations, or grain boundaries.

The crystals were very robust. They were not destroyed when the sample was diluted, indicating that they were not stabilized by a depletion interaction. They also were not destroyed by subjecting them to strong forces induced either with flow, with distortion by indenting the microscope slide near the crystals, or by pulling on one of the particles with laser tweezers. In addition, despite their 2D character, the crystals did not form through interactions at interfaces. They existed as large objects floating freely in the solvent, and they formed equally well in different sample containers and when no interfaces with air were present. Instead, these crystals originated from interactions between the colloidal particles and self-assembled surfactant structures within the fluid.

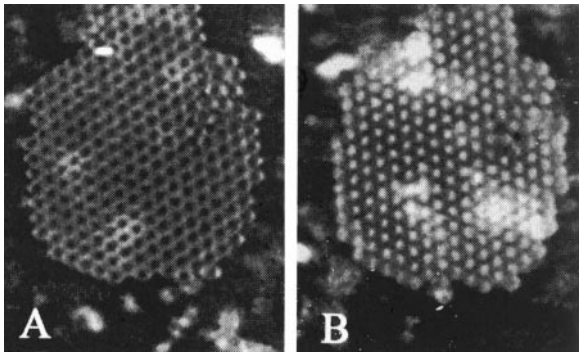

Fig. 2. Images of a 2D colloidal crystal obtained with a laser-fluorescence scanning confocal microscope. The focal planes of the two images are separated by about half of the particle radius, and the same particles are imaged in each picture. (**A**) The edge of the particles and (**B**) their tops.

Coulomb interactions play a critical role in the formation of these crystals. In all of the cases investigated, the total charge in the surfactant was always greater than the total surface charge on the particles when crystals were formed. The particles in the crystals were completely covered by surfactant. This observation was confirmed by adding a fluorescent tag (*14*) that allowed us to identify the precise location of the surfactant, using a laser-fluorescence scanning confocal microscope. In the absence of particles, the fluorescent tag allowed us to identify the vesicles themselves. We show two slices through a 3D image of a crystal (Fig. 2) that were separated by a depth corresponding to the radius of the particles and were fluorescently imaged. In the lower slice (Fig. 2A), the rings are the images of the dye around the edge of the particles, and in the upper slice (Fig. 2B), the round spots are the images of the dye on the top of exactly the same particles. These images show that the particles are completely covered by the surfactant; however, we are unable to determine the thickness of this coverage, because this is below the resolution of the confocal microscope.

Why do 2D rather than 3D crystals form? We investigated the structures initially produced when the particles are first added to the surfactant mixture. At this point, there are many isolated particles and small aggregates of two or three particles. In addition, some larger vesicles are partially covered with a single layer of particles, as shown in Fig. 3, A and B. Typically, less than half the surface area of the vesicle is covered with particles. Interestingly, no additional particles adhered to the bare surface, nor were any of the adsorbed particles ever observed to leave the surface; the adsorption is self-limited. However, once adsorbed, the particles still diffused on the vesicle surface, indicating that the surface was still fluid. Furthermore, the adsorbed particles collected together to form "rafts," which suggests that a weak attractive interaction exists between the particles; this behavior could be caused by the reduction in the fluctuations of the membrane due to the presence of the particles (*15*). There remains a short-range repulsive interaction, which, at least initially, stabilizes the particles; this is confirmed by digitizing images of the rafts and calculating the pair correlation function for the particles, which is liquid-like, with its first peak occurring at the particle diameter (Fig. 4). This indicates that the particle size sets the interaction range. Video tracking of the particle positions shows that their mean-square displacement initially increased linearly with time, as expected for diffusion; however, their maximum displacement was

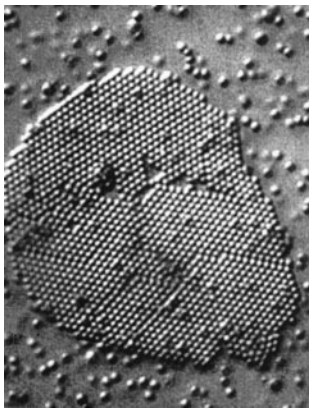

Fig. 1. Shown is a 2D colloidal crystal formed by the interaction of colloidal particles with vesicles of the opposite charge.

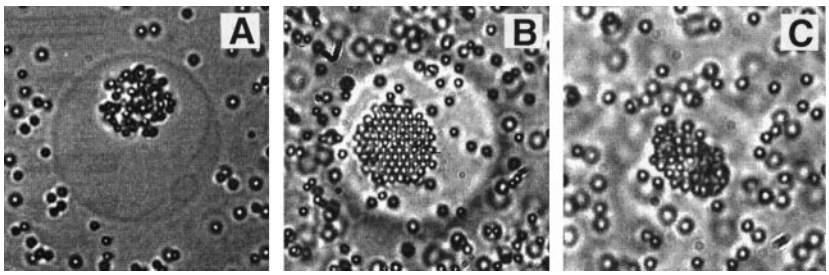

Fig. 3. (**A**) Disordered and (**B**) more ordered rafts of particles adsorbed to the surface of a tense vesicle, seen as the outlines in the picture. The particles in the rafts undergo Brownian motion, restricted by their neighbors. (**C**) Flaccid vesicle covered with particles.

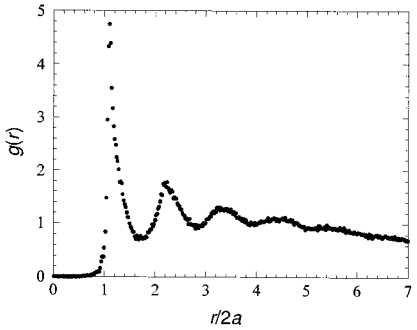

Fig. 4. Pair correlation function, in arbitrary units, for particles on the surface of a vesicle. The peak occurs at the particle diameter, indicating that there is only a very short-range repulsive interaction between the particles.

constrained by their neighbors.

Initially, the rafts of particles remained highly disordered (Fig. 3A). At longer times, they became increasingly ordered (Fig. 3B). Ultimately, the particles would stick permanently to one another and formed robust 2D crystals that could then detach from the vesicles. These observations imply that the sequence of events leading to the formation of these unusual 2D crystals is (i) Coulombic adhesion of particles onto vesicle surfaces, (ii) mutual attraction of the particles on the surfaces, and (iii) fusion of the bilayers on each particle to form the robust colloidal crystals.

We propose a model that accounts for the initial adsorption of the negatively charged colloidal particles on the positively charged vesicles. These vesicles may initially not be completely tense and spherical. The Coulomb attraction causes particles to stick to vesicles with at least a fraction of their surface in close contact with vesicular membranes. The positive vesicle charges neutralize negative particle charges, which release their associated counterions and allow them to escape. However, because the interior is enclosed, counterions cannot escape from within the vesicle; nevertheless, they can migrate laterally to a portion of the vesicle not in contact with particles where they can neutralize an exterior vesicle charge and allow its counterion to escape (*16*). In addition, because the membrane is composed of a mixture of neutral and charged surfactants, demixing can occur, enriching the charged surfactant in regions of the surface covered with particles. The result is the total neutralization of particle charge in contact with membrane. Moreover, the lateral charge migration can reverse the charge elsewhere on the membrane and prevent further particle adsorption (*16*). Thus, the adsorption is self-limited; this accounts for the observation of vesicles partially covered by "rafts," with no further particle adsorption. Detailed calculations (*16*) support this scenario.

Although the Coulomb interaction sets the membrane area in contact with particles, A_1, it does not determine the number of adsorbed particles, N. There could be a small number of particles completely covered with membrane or a large number of particles only partially covered with membrane. Instead, once A_1 is fixed, N is determined by constraints on the total vesicle area available for particle contact and by the existence of a line tension Γ for interfaces that separates charge-rich surfactant regions in particle contact and charge-depleted regions not in particle contact. Line tension disfavors interfaces and thus favors having all of the particles completely covered, which could leave zero interfacial length (Fig. 5). Therefore, in the absence of other effects, there would be $N = A_1/4\pi r^2$ particles of radius r adsorbed on a vesicle of area A. This value of N cannot always be reached; for example, it is impossible for a tense spherical vesicle, with volume $V = 4\pi/3R_0^3$ and area $A_0 = 4\pi R_0^2$, to wrap more than an infinitesimal area of each particle without rupture. Thus, in this limit, a large number of particles is needed to reach a total adhering area of A_1. More generally, N is determined by both A_1 and the vesicle area excess, $\Delta = A - 4\pi R_0^2$. If $\Delta > A_1$, there will be $N = A_1/4\pi r^2$ completely wrapped particles, and because not all of the excess area has been used, the resultant vesicle will be flaccid. Consistent with this model, we observed some flaccid, particle-covered vesicles (Fig. 3C). If $\Delta < A_1$, there will be $N = A_1^2/(4\pi r^2\Delta)$ partially covered particles (Fig. 5) adsorbing all excess area, and the resultant vesicle will be tense. Consistent with this model, we observed some tense, spherical vesicles that are partially covered with particles (Fig. 3, A and B); it is only these tense vesicles that produce 2D colloidal crystals.

This surface-mediated crystallization on vesicles combines surfactant structures with Coulombic attraction. A wide variety of other self-assembled surfactant structures can be formed, and many of these may also lead to novel routes to colloidal crystallization. In addition, the attractive interactions and the dynamics of the particles on the surface of vesicles provide a convenient means of studying the behavior of particles adsorbed on fluid membranes; this may provide a useful model system for the study of other biologically important structures such as the properties of proteins on cell membranes (*17*). Finally, these interactions between colloidal particles and surfactant structures provide a novel form of colloidal crystallization that may find important applications in the use of colloidal particles as templates for new structures.

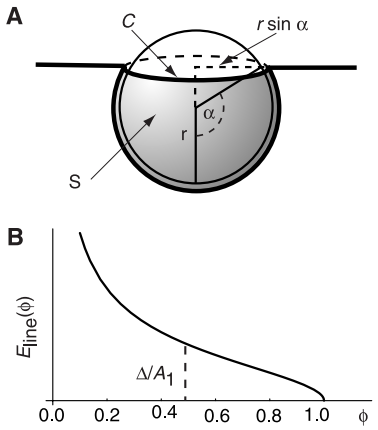

Fig. 5. (**A**) A particle of radius r wrapped to angle α by the vesicle membrane. The area of the particle in contact with the membrane (shaded region of figure) is $a = 2\pi r^2(1 - \cos\alpha)$ so that the fractional area covered is $\phi = (1 - \cos\alpha)/2 \leq 1$. The length of the interface that separates charged membrane in particle contact from less-charged membrane not in particle contact is $C = 2\pi r\sin\alpha$. The total area covered by N particles wrapped in this way is $4\pi r^2 N\phi$ and is equal to A_1. The excess membrane area used by each particle is the difference between a and the area $\pi r^2\sin^2\alpha$ of the circular cross section at angle α. Thus, the total excess area used by N particles is $4\pi r^2 N\phi^2$, which is equal to the total available excess area, Δ, when $\Delta \leq A_1$, that is when $\phi \leq 1$. When $\Delta > A_1$, not all excess membrane area is used to wrap particles, and all of the particles are completely engulfed ($\phi = 1$). (**B**) Plot of the line tension energy $E_{line}(\phi) = N\Gamma C = (A_1\Gamma/r)\sqrt{(1/\phi - 1)}$ as a function of ϕ for fixed A_1. This is a monotonic decreasing function of ϕ. The lowest energy configuration is that with the largest value of ϕ consistent with constraints. When $\Delta \leq A_1$, then from (a) above $\phi \leq \Delta/A_1$. When $\Delta > A_1$, $\phi = 1$. Thus, the minimum energy corresponds to $\phi = \min(1, \Delta/A_1)$. When $\Delta > A_1$ and $\phi = 1$, $N = A_1/4\pi r^2$. When $\Delta \leq A_1$, $\phi = \Delta/A_1$, as indicated by the dotted line in the figure, and $N = A_1^2/(4\pi r^2\Delta)$.

References and Notes

1. P. Yang *et al.*, *Science* **282**, 2244 (1998).
2. B. T. Holland, C. F. Blanford, A. Stein, *Science* **281**, 538 (1998).
3. J. E. G. J. Wijnhoven and W. L. Vos, *Science* **281**, 802 (1998).
4. A. A. Zakhidov *et al.*, *Science* **282**, 897 (1998).
5. K. Wong, B. Cabane, R. Duplessix, P. Somasundaran, *Langmuir* **5**, 1346 (1989).
6. J. O. Rädler, I. Koltover, T. Salditt, C. R. Safinya, *Science* **275**, 810 (1997).
7. I. Koltover, T. Salditt, J. O. Rädler, C. R. Safinya, *Science* **281**, 78 (1998).
8. The cmc's are 0.15 mM for DDAB and 0.24 mM for TX.
9. M. Dubois, T. Gulik-Krzywicki, B. Cabane, *Langmuir* **6**, 673 (1993).
10. K. Beyer, *J. Colloids Interface Sci.* **86**, 73 (1982).
11. J. Oberdisse *et al.*, *Langmuir* **12**, 1212 (1996).
12. Spheres were obtained from Interfacial Dynamics Corp: 0.83-μm diameter with measured zeta potential of −45 mV, coated with sulfate and carboxylate groups; 0.98-μm diameter, −15 mV, sulfate groups; 1.0-μm diameter, −15 mV, combination of sulfate and amine groups. Polydispersities of all particles were less than 5% in radius.
13. Intermediate values: $0.5 < x < 0.87$ for the carbox-

ylate/sulfate particles and $0.12 < x < 0.87$ for the sulfate particles.
14. The fluorescent tag was 5-dodecanoyl-aminofluorescein, at a concentration of 2% of total surfactant.
15. M. Goulian, R. Bruinsma, P. Pincus, *Europhys. Lett.* **22**, 145 (1993).
16. H. Aranda-Espinoza *et al.*, *Science* **285**, 394 (1999).
17. I. Koltover, J. O. Rädler, C. R. Safinya, *Phys. Rev. Lett.* **82**, 1991 (1999).
18. We thank J. Crocker and E. Weeks for assistance with particle tracking. Supported by the Materials Research Science and Engineering Center Program of NSF under award number DMR96-32598, and by NSF through equipment grants DMR97-24486 and DMR97-04300. L.R. also acknowledges support from the bourse Lavoisier du Ministère Français des Affaires Etrangères. N.D. was supported in part by NSF grant CTS-9814398; P.N. was supported in part by NSF grant DMR98-07156.

12 August 1999; accepted 28 October 1999

Postnatal Sex Reversal of the Ovaries in Mice Lacking Estrogen Receptors α and β

J. F. Couse,[1] S. Curtis Hewitt,[1] D. O. Bunch,[2] M. Sar,[3] V. R. Walker,[1] B. J. Davis, [4] K. S. Korach[1]*

Mice lacking estrogen receptors α and β were generated to clarify the roles of each receptor in the physiology of estrogen target tissues. Both sexes of αβ estrogen receptor knockout (αβERKO) mutants exhibit normal reproductive tract development but are infertile. Ovaries of adult αβERKO females exhibit follicle transdifferentiation to structures resembling seminiferous tubules of the testis, including Sertoli-like cells and expression of Müllerian inhibiting substance, sulfated glycoprotein-2, and *Sox9*. Therefore, loss of both receptors leads to an ovarian phenotype that is distinct from that of the individual ERKO mutants, which indicates that both receptors are required for the maintenance of germ and somatic cells in the postnatal ovary.

Reports of estrogen synthesis in the fetal ovaries of several species suggest the involvement of the estrogen signaling system in ovarian development (*1*). Insights into the physiological roles of estrogen have been gained from the study of mice lacking the capability to synthesize either estradiol (ArKO mice) (*2*) or one of the two cognate estrogen receptors (ERs) ERα (αERKO) and ERβ (βERKO) (*3*). However, conclusions drawn from these mutant mice are confounded by possible compensatory mechanisms provided by (i) the opposite ER in each respective ERKO mutant or (ii) maternal estrogens during gestation or estradiol-independent ER actions in the ArKO mutant, or both. Therefore, to further elucidate the role of estrogen signaling in reproductive tract development and function, mice homozygous for a targeted disruption of both ER genes (*Estra* and *Estrb*), termed αβERKO mice, were generated (*4*). Adult (2.5 to 7 months) αβERKO mice of both sexes survive to adulthood and exhibit no marked abnormalities as compared to control littermates, thereby challenging earlier speculations that the ER is essential to survival (*5*).

αβERKO males are infertile but possess a grossly normal reproductive tract, in agreement with past evidence that estradiol is unnecessary for the development of male gonads and reproductive structures. The testes of adult (2.5 to 7 months) αβERKO males exhibited various stages of spermatogenesis, yet the numbers and motility of epididymal sperm were reduced by approximately 80 and 5%, respectively (Fig. 1). This phenotype is similar to that of the αERKO male and is therefore characteristic of the loss of ERα; it does not occur in βERKO males, which exhibit normal fertility (*3*) and sperm counts (Fig. 1E). The αβERKO testicular phenotype also does not resemble that reported in ArKO mice, which exhibit arrested spermatogenesis but no αERKO-like tubule dysmorphogenesis (*2*). This discrepancy between male mice lacking estradiol and those lacking both ERs suggests the existence of undocumented aromatase- or ER-encoding genes or estradiol-independent ER actions within the male reproductive tract (or both).

In agreement with classical fetal castration studies indicating that differentiation of the female genital ducts is independent of ovarian steroids (*6*), αβERKO females exhibit proper differentiation of the Müllerian-derived structures (the uterus, cervix, and upper vagina). The functional uterine compartments are present in the uteri of αβERKO females, yet the dependency of each on estradiol for postnatal growth is definitively illustrated by their severe hypoplasia in adult (2.5 to 7 months) αβERKO females (Fig. 2, A and B). Similar uterine hypoplasia occurs in αERKO but not in βERKO females (*3*), which corresponds to reports of ER localization and is characteristic of the loss of

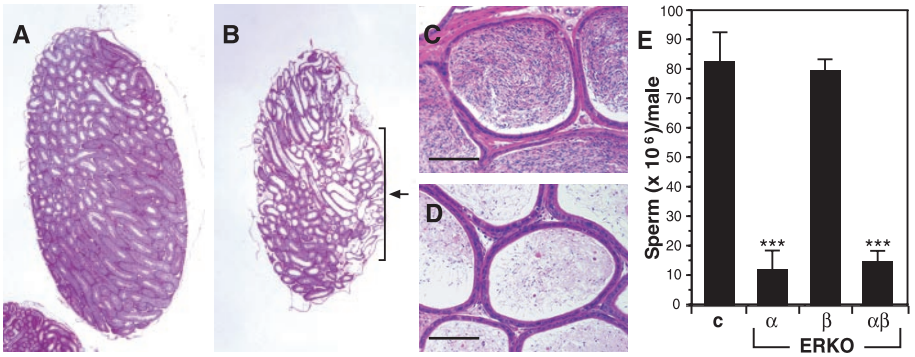

Fig. 1. Morphological and functional phenotypes of the αβERKO male reproductive tract. Testes were fixed overnight in cold Bouin's fixative, passed through several changes of cold water over 2 days, transferred to cold 50% ethanol for 24 hours, and then immersed in cold 70% ethanol until paraffin embedding. Shown are 5-μm sections stained with hematoxylin and eosin (H&E). Low-power magnification of a testis from a representative age-matched (**A**) control male and (**B**) an αβERKO adult male (2.5 to 7 months) illustrates the luminal swelling and loss of germinal epithelium of the seminiferous tubules in the αβERKO testis, which is most evident along the region indicated by the arrowed bracket. High-power (×66) magnification of the caudal epididymis of a representative (**C**) wild-type male and (**D**) of an αβERKO adult male illustrates the reduced density of the sperm population in the αβERKO male. (**E**) Epididymal sperm counts carried out as previously described (*25*) on males ≥100 days old indicate the significant reduction in sperm number in the αβERKO male that is characteristic of that observed in age-matched αERKO males. For control (c), αERKO, and βERKO, mice, $n = 4$ animals analyzed; for αβERKO mice, $n = 5$ animals analyzed. Scale bar, 100 μm. ***ANOVA, $P < 0.001$.

[1]Receptor Biology Section, Laboratory of Reproductive and Developmental Toxicology, [4]Laboratory of Experimental Pathology, National Institute of Environmental Health Sciences, National Institutes of Health, Research Triangle Park, NC 27709, USA. [2]Laboratory of Reproductive Biology, Department of Cell Biology, University of North Carolina at Chapel Hill, Chapel Hill, NC 27599, USA. [3]Chemical Industry Institute of Toxicology, Research Triangle Park, NC 27709, USA.

*To whom correspondence should be addressed. E-mail: korach@niehs.nih.gov